Indian Journal of Chemical Technology
Vol. 32, November 2025, pp. 734-748
DOI: 10.56042/ijct.v32i6.19821

Surfactant-assisted synthesis of Cu-Doped Co_3O_4@carbon nano flake nanocomposites for effective photocatalytic breakdown of brilliant green dye under UV irradiation

Chandrakala Vinayagasundaram & Arputharaj Samson Nesaraj*

Centre for Smart Electrochemical Energy Conversion Systems, Department of Chemistry, School of Advanced Sciences, Kalasalingam Academy of Research and Education (Deemed to be University), Anand Nagar, Krishnankoil - 626 126, Tamil Nadu, India

*E-mail: samson@klu.ac.in

Received 18 May 2025; accepted 8 October 2025

This study explores the fabrication, characterization, and photodegradation efficiency of Cu-doped Co_3O_4 (0–50 mol%) incorporated into a carbon nano flake (CNF) composite for the removal of brilliant green dye. The synthesized materials have been analyzed using XRD, SEM-EDAX, TEM, UV-DRS, and XPS, confirming an FCC crystalline structure with irregular spherical grains. Under UV light irradiation, Cu-doped $Co_3O_4$and Cu-doped Co_3O_4@CNF achieved 91.8% and 98.4% dye removal within 40 min. The improved efficiency is attributed to the effective role of Co_3O_4 nanoparticles in reducing electron-hole recombination, enhancing photocatalytic activity and promoting the degradation of organic pollutants in wastewater treatment applications.

Keywords: Brilliant Green, CNF nanocomposite, Cu-doped Co_3O_4, Photodegradation, Reusability

Water serves as a vital necessity for all life forms inhabiting our planet. However, the existence of water pollutants poses a significant hazard to organisms residing in both aquatic and terrestrial environments. Among the myriads of environmental pollutants, dyes emerge as a prominent contributor to pollution, endangering the well-being of aquatic and terrestrial biota alike[1]. Brilliant green (BG) is a cationic dye generally employed as a biotic tinge, poultry feed additive, wound healing agent and animal drug to prevent the growth of intestinal parasites, fungi and mold[2]. BG dye exhibits high toxicity not only to humans but also to aquatic ecosystems and gram-positive bacteria. Consequently, it is crucial to degrade toxic synthetic dyes such as BG before they are released into the environment.

Hence, scientists have been actively involved in devising efficient, cost-effective, and eco-friendly approaches to detect and evacuate harmful dyes. Various physicochemical and microbiological treatment techniques, including photocatalysis[3], nanofiltration[4], microwave[5, 6], adsorption[7], electrocoagulation[8], Fenton[9], and bio methods, have been explored for the efficient purification water contaminated with dye molecules. Among these methods, photocatalysis has proven to be particularly effective and economical.

A number of studies have demonstrated that transition metal oxide nanoparticles are effective for treating wastewater containing harmful dyes[10-14]. This is attributed to their expansive surface area and semiconductor characteristics[15]. Transition metal based materials, viz., cobalt and cobalt oxide[16,17], iron and iron oxide[18], copper and copper oxide NPs[19], etc. have been extensively studied. Notably, Co and Co_3O_4 have showcased remarkable versatility, being utilized extensively as gas sensors, catalysts, pigments, advanced energy storage materials and magnetic compounds[20, 21].

A wide range of fields have shown great interest in cobalt oxides, which are among the most important transition metal oxides. Photocatalytic dye degradation can be achieved with cobalt oxide nanoparticles, which are excellent semiconductor materials with enough band holes[22-25]. As electron-hole pairs recombine rapidly during photocatalysis, dye degradation is sometimes limited. To address this and improve the catalytic performance of these materials, researchers have explored doping with graphene, polymers, carbon, metals and carbon contained materials like g-C_3N_4, CNF and CNT. These additives typically modify the absorption spectrum of metal oxides, facilitating a shift from the

limited UV range to a broader visible range[26, 27]. The incorporation of metal dopants into cobalt oxide provides an effective method of improving and regulating its morphology. Advances in applications like the photocatalytic eviction of various pigments can be achieved by doping metal like Cu[28, 29].

Hence, a multitude of techniques has been documented in this domain for the fabrication of Co_3O_4 nanoparticles, encompassing sol-gel, thermal decomposition, reduction/oxidation routes, chemical spray pyrolysis, hydrothermal, microemulsion, hard templating, solvothermal, mechanochemical, chemical combustion methods and metal-organic chemical vapour deposition[30]. Each of these physical and chemical methods requires specific instrumentation and often entails harsh conditions. However, we present a simple precipitation method that offers greater ease, simplicity, and effectiveness in synthesizing Co_3O_4 nanoparticles.

In this study, we propose the development of photocatalysts by doping various concentrations of copper onto cobalt oxide nanoparticles. All the materials are prepared by a simple co-precipitation method. These nanoparticles were then supported by CNF particles. The structural, morphological, and elemental and optical properties were examined using XRD, SEM-EDAX, TEM, UV-DRS, and XPS. Moreover, we carried out a comprehensive examination of the catalytic performance of the produced materials, considering diverse parameters including pH, time, dosage, and concentration of dye. These results lay the groundwork for future investigations into the economical synthesis and application of nanomaterials for dye eviction via photodegradation.

Experimental section

Cobalt acetate tetrahydrate ($Co(CH_3COO)_2{\cdot}4H_2O$), copper sulphate pentahydrate ($CuSO_4.5H_2O$), Urea (CH_4N_2O), Glucose ($C_6H_{12}O_6$), double distilled water, sodium hydroxide (NaOH) and brilliant green dye. This study utilized high-purity analytical-grade chemicals.

Fabrication of Co_3O_4 nanoparticles

Cobalt oxide nanoparticles were fabricated through a straightforward soft chemical technique. Initially, a 0.1 M solution of ($Co(CH_3COO)_2{\cdot}4H_2O$) (100 mL) was stirred for minimum 20 min. To this copper acetate solution, a 0.2 M of NaOH (100 mL) and 10 mL of CTAB solution was added, and then continuously mixed for 3 h. A light reddish precipitate formed, which was extensively rinsed with a 9:1 (v/v) water/ethanol solution to eliminate any contaminants. The obtained residue was dehydrated at 80°C for about 1 h, and then calcined at 400°C for 5 h to remove hydroxyl groups, ultimately yielding the final product. For the preparation of doped nanoparticles, a similar process was used, with the addition of ($CuSO_4{\cdot}5H_2O$) at concentrations of 10 to 50 mol% alongside ($Co(CH_3CO_2)_2{\cdot}4H_2O$). The materials were named as Co_3O_4 doped with 10 mol% Cu(CuCo1), Co_3O_4 doped with 20 mol% Cu (CuCo2), Co_3O_4 doped with 30 mol% Cu (CuCo3), Co_3O_4 doped with 40 mol% Cu (CuCo4) and Co_3O_4 doped with 50 mol% Cu (CuCo5)[26]. The flow chart to prepare Cu-doped Co_3O_4 nanoparticles is shown in Fig. 1.

Preparation of carbon nano flake (CNF) particles

Glucose and urea in a 1:1 ratio were dispersed in water and mixed well at 50°C for about 10 min until a gel-like substance formed. The formed gel was introduced into a furnace maintained at 500°C, producing a black, porous foam-like material. The foam was then finely crushed to get refined powder of carbon nano flake (CNF) particles, which were later used for the synthesis of metal doped nanocomposite material[26].

Preparation of Cu-doped Co_3O_4@CNF nanocomposite

A facile co-precipitation technique was employed to synthesize Cu-doped Co_3O_4@CNF nanocomposites. Solutions of 0.07 M ($Co(CH_3COO)_2{\cdot}4H_2O$) and 0.03M $CuSO_4{\cdot}5H_2O$, each in 100 mL volumes, were prepared independently and then combined in a 500 mL beaker. The mixture was stirred for 20 min on a stir plate, during which 10mL of CTAB surfactant solution was introduced. After adding the CNF particles, stirring continued for 15 min more. Subsequently, a 0.04 M sodium hydroxide solution was gradually added with continuous stirring, which was maintained for an

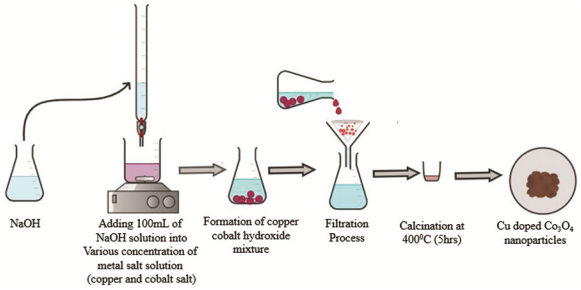

Fig. 1 — Flow chart to prepare Cu-doped Co_3O_4 nanoparticles

additional three hours. The resulting black precipitate was thoroughly washed with water/ethanol to eliminate impurities. The obtained material was first dried in an oven at 80°C, followed by calcination at 300°C for five hours to eliminate OH radicals, ultimately producing the final compound identified as 40 mol% Co_3O_4@CNF (CuCo4@CNF)[26].

Characterization of prepared photocatalysts

The crystalline structure of the synthesized material was analysed using Powder XRD with a Bruker D8 Advance ECO system equipped with CuKα radiation (λ = 1.54056 Å). The surface morphology was studied through SEM using a ZEISS-EVO 18, while the atomic composition and purity were assessed via XPS using a PHI 5000 Versa Probe III. UV-Vis diffuse reflectance spectroscopy (DRS) measurements were performed using a Shimadzu UV-2450 spectrophotometer, whereas the degradation efficiency of the solutions was evaluated with a Shimadzu UV-1800 spectrophotometer. Additionally, a Heber multi-lamp photoreactor (model HML-MP 88) emitting at 365 nm was used to facilitate the decomposition of organic contaminants[26].

Photocatalytic degradation of BG dye using synthesized catalysts

The effectiveness of the synthesized photocatalysts in degrading BG dye was assessed using a Heber multi-lamp photoreactor. In the degradation study, 50 mg of the catalyst was introduced into 100 mL of a 10 ppm BG dye solution contained in a 200 mL beaker. To confirm adsorption-desorption equilibrium, the mixture was continuously stirred in a dark environment for 30 min before initiating the photocatalytic reaction. The degradation process was then carried out in a reaction chamber under UV light exposure. To monitor the concentration changes of BG, approximately 3 mL of the reaction mixture was collected every 5 min, followed by centrifugation. The change in absorbance at 625 nm was monitored using a UV-visible spectrophotometer to track the degradation process. After the irradiation period, the catalyst was recovered and analyzed to evaluate its stability. The extent of dye removal was determined using the corresponding degradation formula outlined in Eq. (1)[31].

$$\% \text{ of dye degradation} = (C_o - C_t) / (C_o) \text{ X } 100 \quad \ldots(1)$$

In this context, C_o refers to the initial concentration, while C_t represents the dye solution concentration at a specific time t.

Results and Discussion

Characterisation of the nanocomposites

Analyses of X-ray diffraction were carried out on prepared nanoparticles to investigate their crystalline structure. Fig. 2a shows the XRD pattern obtained on Cu doped Co_3O_4.The Co_3O_4 displayed sharp, narrow peaks at 2θ angles of 18.90, 31.14, 36.68, 38.51, 44.68, 55.75, 59.31, and 65.10, correlate to the diffraction planes (111), (220), (311), (222), (400), (422), (511), and (440). It is evident from these peaks that the material satisfies to the Fd3m space group and has a FCC spinel structure. A diffraction peak from CoO or any other phase is not observed, thus confirming that phase-pure Co_3O_4 is formed. In accordance with the JCPDS No. 76-1802 standard, this approach is appropriate[32].Therefore, it can be inferred that Cu ions are directly incorporated into the Co_3O_4 lattice without disrupting its crystal structure. However, in the CuCo5 sample, an additional peak

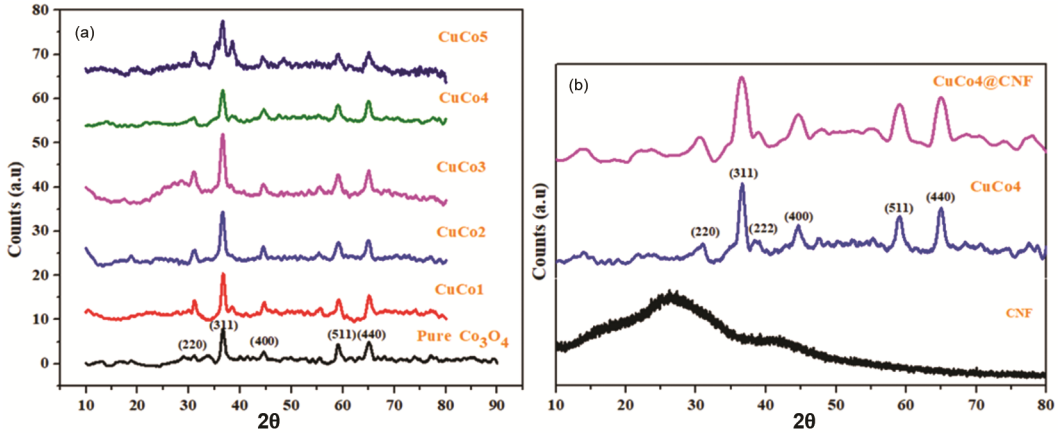

Fig. 2 — X-ray diffraction patterns of (a) pure Co_3O_4 and various amount of Cu doped Co_3O_4 and (b) CNF, CuCo4 and CuCo4@CNF nanocomposite

appeared, possibly suggesting the presence of excess copper at higher concentrations. The average crystallite size was measured using Debye-Scherrer's Eq. (2).

$$D = K \lambda / \beta \cos \theta \quad \ldots(2)$$

Here, λ represents the wavelength, β denotes the full width at half maximum (FWHM), and θ is the diffraction angle. The average crystallite sizes for pure Co_3O_4, CuCo1, CuCo2, CuCo3, CuCo4, and CuCo5 were determined to be 7.31 nm, 12.92 nm, 11.07 nm, 5.28 nm, 10.19 nm, and 7.31 nm, respectively. Sharp diffraction peaks were observed in Fig. 2a for all synthesized materials. However, in Fig. 2b, slightly broader peaks appeared in CuCo4@CNF, suggesting that Cu-doped Co_3O_4 is distributed on the surface of the carbon nanoflakes, leading to reduced peak intensity. The medium crystallite size of the synthesized CuCo4@CNF was found to be 12.72 nm.

SEM coupled with EDS was employed to analyse the surface pattern of pure Co_3O_4, pure CNF, as well as various percentages of Cu-doped Co_3O_4 and Cu-doped Co_3O_4@CNF nanocomposites and the images were illustrated in Fig. 3(a-i).

SEM analysis of the samples revealed that they have evenly distributed irregular sphere shaped grains. There was no difference in the morphology of all samples, but some nanocomposites exhibited agglomeration, likely since smaller particles clustered together[31]. The thin, flake-like structure of CNF is clearly shown in Fig. 3(g-h). The thin, flake-like structure of CNF is distinctly visible in Fig. 3 (g-h). In Fig. 3 (i), SEM images of the Cu-doped Co_3O_4@CNF nanocomposite illustrate the distribution of Cu-doped Co_3O_4 nanoparticles across the flake-like matrix of CNF particles.

Quantitative chemical composition analysis through EDAX for pure Co_3O_4, CNF, and different ratios of Cu-doped Co_3O_4 and Cu-doped Co_3O_4@CNF nanocomposites confirmed the evenly distribution of Cu, Co, O, and C elements (Fig. 4). Additionally, colour mapping analysis of the CuCo4@CNF nanocomposite demonstrated the even dispersion of atoms across the surface of the CNF-based nanocomposite. Additionally, the weight percentages of copper, cobalt, oxygen and carbon in all the synthesized nanoparticles were determined through EDAX analysis. It is shown in Table 1.

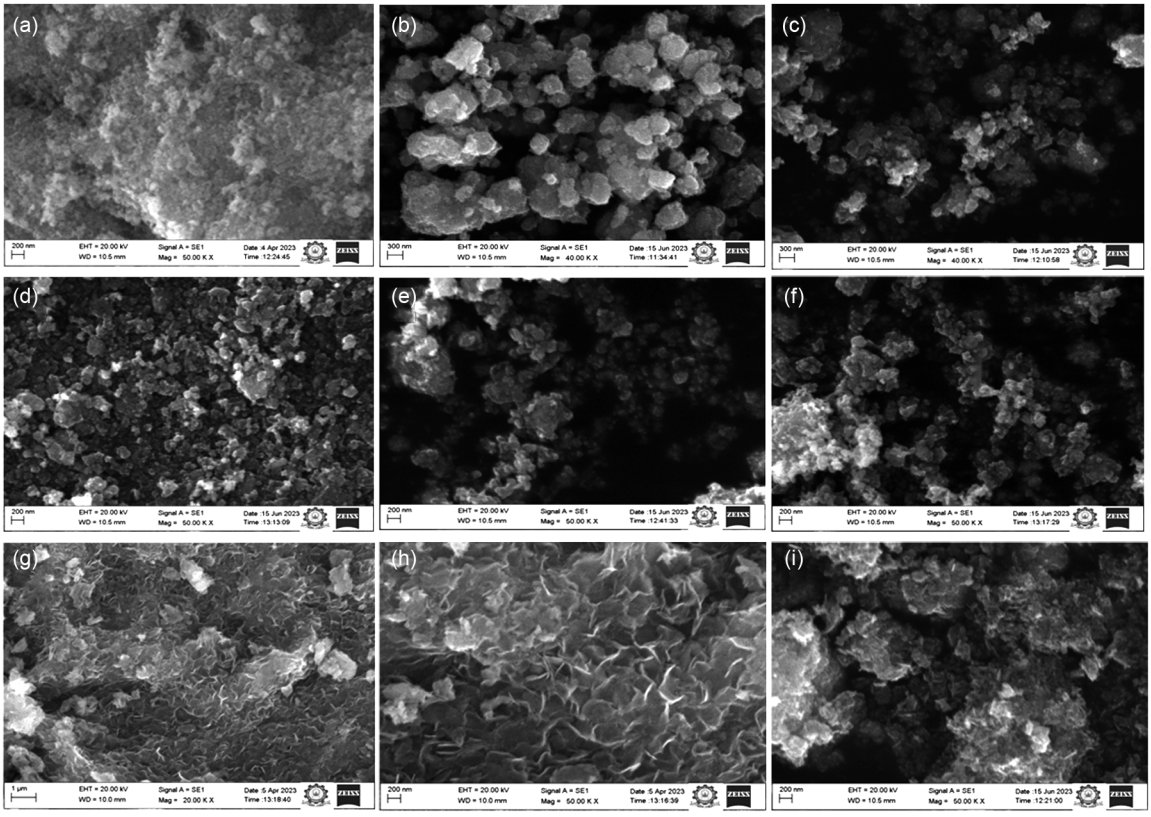

Fig. 3 — SEM photographs of (a) Pure Co_3O_4, (b) CuCo1, (c) CuCo2, (d) CuCo3, (e) CuCo4, (f) CuCo5, (g) Pure CNF (1µm), (h) Pure CNF (200nm), and (i) CuCo4@CNF

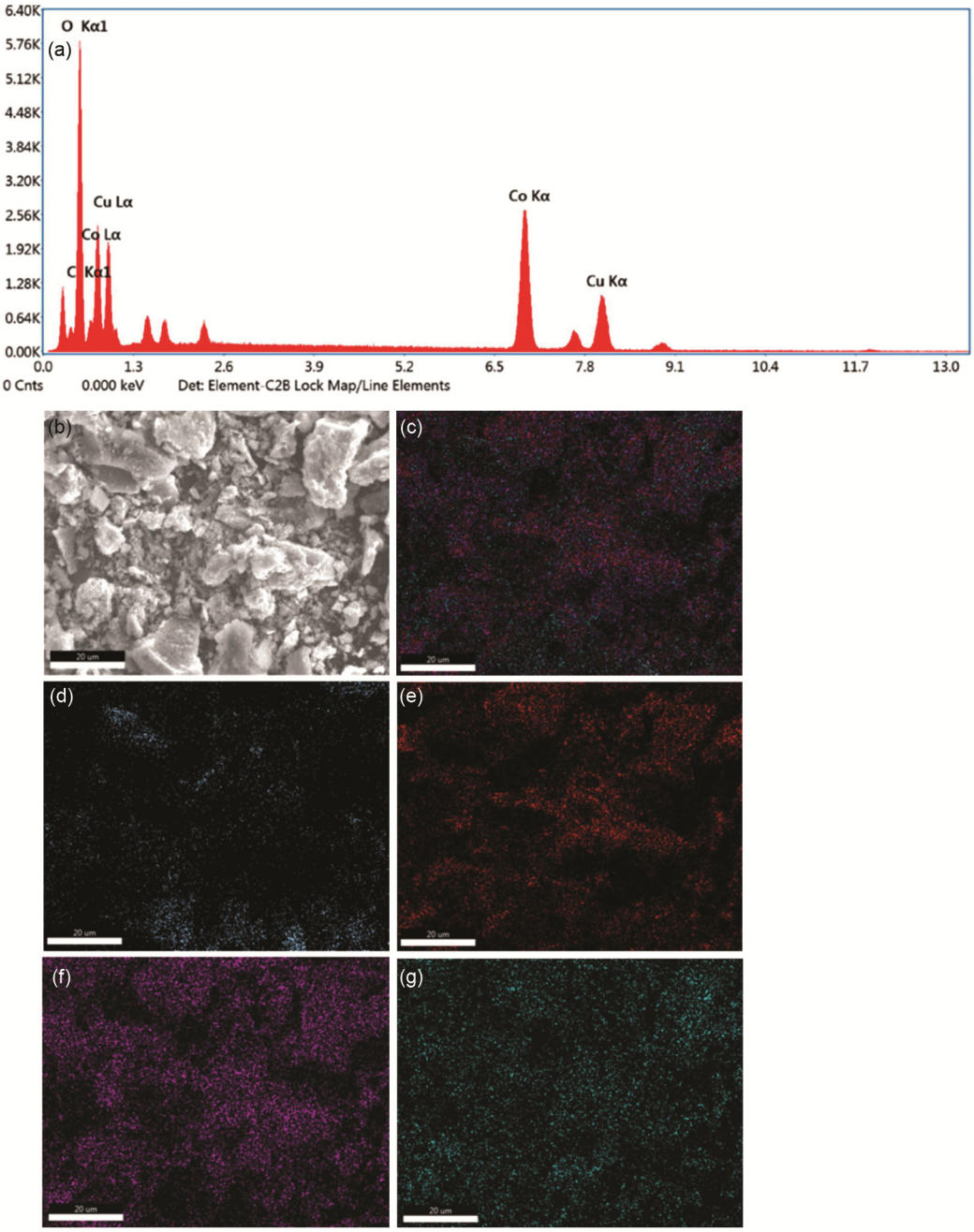

Fig. 4 — (a) EDAX of CuCo4@CNF, (b) Detailed colour map of CuCo4@CNF, Colour mapping image of, (c) CuCo4@CNF, (d) Carbon element, (e) Oxygen element, (f) Cobalt element and (g) Copper element

Fig. 5 shows the transmission electron microscopy (TEM) analysis of the CuCo4@CNF, which reveals well-dispersed nanoparticles with an average size of 7.64 nm, as observed in both high- and low-magnification. The selected area electron diffraction (SAED) pattern confirms the polycrystalline nature of the material, with distinct crystalline rings characteristic of copper-doped cobalt oxide phases, in line with previous studies on such nanostructures. The particle size distribution is relatively narrow, with most particles ranging from 6–9 nm, suggesting effective control during synthesis and potential for enhanced catalytic activity. The overall results indicate that the copper and cobalt oxides are successfully doped and uniformly anchored on the CNF matrix.

Fig. 6 presents the XPS spectra of the CuCo4@CNF nanocomposite. As illustrated in

Table1 — Elemental detailing of prepared materials

S. No	Name of the sample	Cobalt (Co)		Copper (Cu)		Oxygen (O)		Carbon (C)	
		Wt (%)	At (%)	Wt (%)	At (%)	Wt (%)	At(%)	Wt (%)	At (%)
1	Pure Co_3O_4	75.9	46.1	-	-	24.1	53.9	-	-
2	CuCo1	64.9	37.5	7.7	4.1	27.4	58.3	-	-
3	CuCo2	58.4	34.0	14.4	7.8	27.2	58.2	-	-
4	CuCo3	58.2	38.0	21.5	13.0	20.4	49.0	-	-
5	CuCo4	42.6	24.3	28.4	15.0	28.9	60.7	-	-
6	CuCo5	37.0	21.9	36.5	20.1	26.5	58.0	-	-
7	Pure CNF	-	-	-	-	-	-	100.0	100.0
8	CuCo4@CNF	38.1	17.5	23.3	9.9	26.0	37.9	44.0	12.7

Note: Wt* (Weight), At* (Atomic)

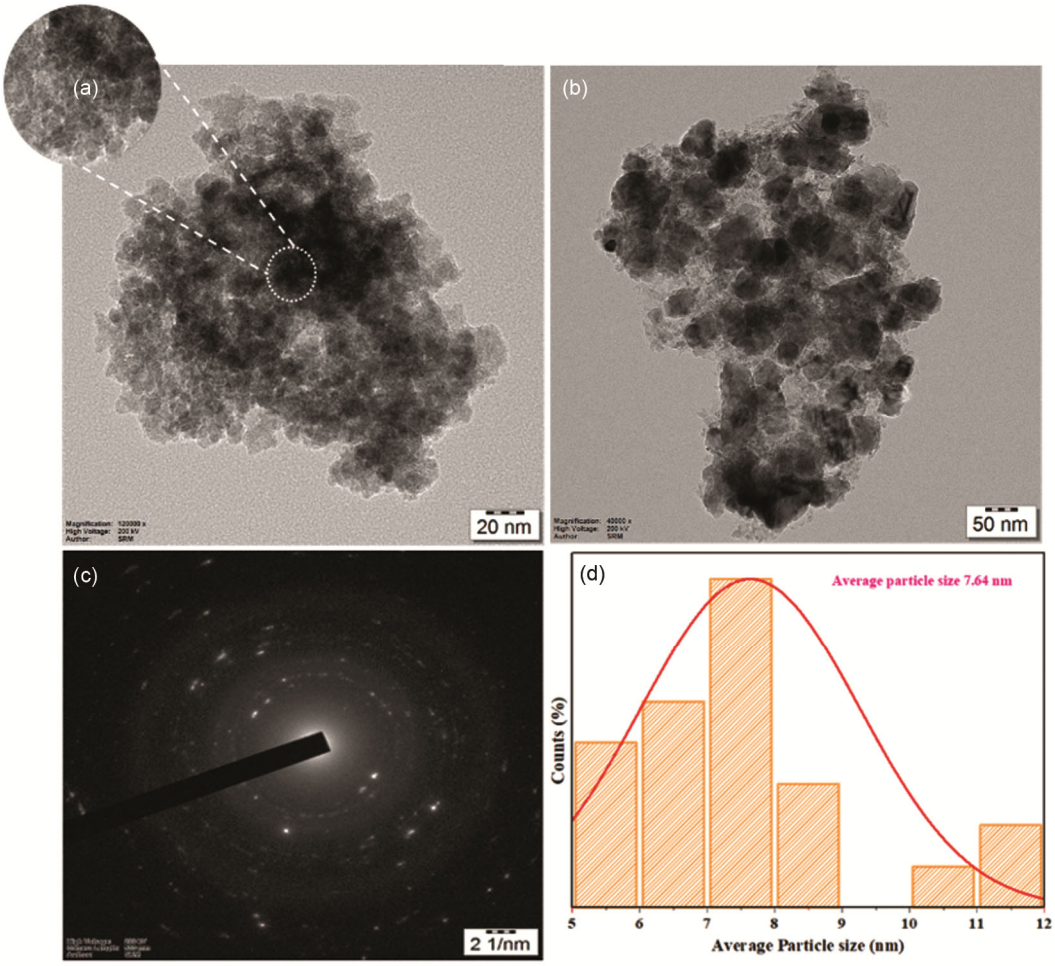

Fig. 5 — (a-b) TEM image of CuCo4@CNF, (c) SAED pattern of CuCo4@CNF and (d) histogram of CuCo4@CNF

Fig. 6a, the patterns indicate the occurrence of C, O, Cu and Co. Fig. 6b presents two significant peaks in the O 1s spectrum: the peak at 529.5 eV relates to surface-adsorbed oxygen, while the peak at 531.2 eV is attributed to metal-O bonds[33, 34]. The XPS spectra of the Cu 2p core level for the nanocomposites are indicated in Fig.6c. In Fig. 6c, the Cu 2p core level XPS spectrum of the doped sample exhibits Cu 2p signals at 933.8 eV and 954 eV, relating to Cu $2p^{3/2}$ and Cu $2p^{1/2}$, respectively. Further, peaks at 942.3 eV and 962.4 eV are linked to strong Cu^{2+} satellite signals[35]. Fig. 6d illustrates the Co 2p spectrum, where peaks at 780.1 eV and 795.5 eV relate to Co $2p_{3/2}$ and Co $2p_{1/2}$, respectively. These peaks can be further deconvoluted to reveal the Co^{3+} state at 786.3 eV and the Co^{2+} state at 803.8 eV[36, 37]. Additionally,

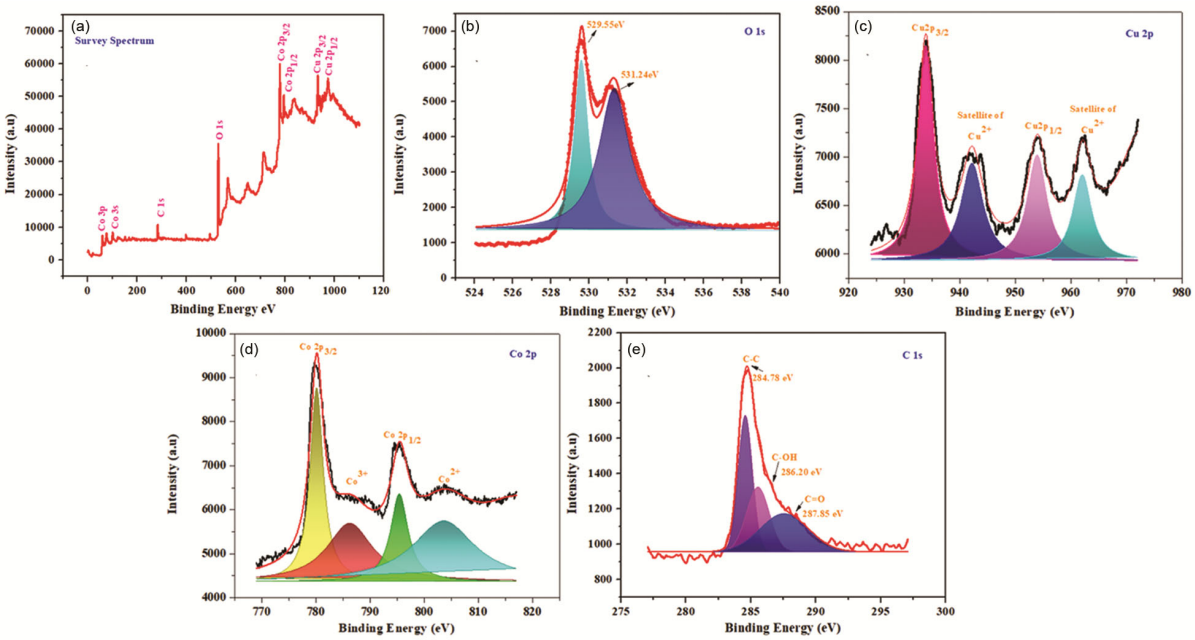

Fig. 6 — (a-e) XPS spectra of CuCo4@CNF nanocomposite

Fig. 6e highlights the binding energies for C 1s, originating from the CNF particles.

The optical characteristics of the synthesized materials were analyzed through UV-DRS spectroscopy, as illustrated in Fig. 7. These characteristics provide valuable information on magnetic excitations, impurity levels, and related phenomena[38]. The E_g of the prepared photocatalyst was found out by Tauc's Equation as follows.

$$\alpha h\nu = A\,(h\nu - E_g)^n \quad \ldots(3)$$

Here, E_g represents the bandgap, hvh\nuhν denotes the photon energy, and A is a constant used in the calculation. The parameter n defines the type of electronic or optical transition occurring within the material, with possible values of 1/2, 2, 3/2, or 3[32, 39]. The bandgap E_g values were determined from the plots of $(\alpha h\nu)^{1/2}$ versus $h\nu$, yielding 2.17 eV, 2.15 eV, 2.14 eV, 2.12 eV, 2.09 eV, 2.11 eV, and 2.06 eV for Pure Co_3O_4, CuCo1, CuCo2, CuCo3, CuCo4, CuCo5, and CuCo4@CNF, respectively. It was observed that the bandgap underwent a slight shift due to the influence of Cu concentration, with the maximum bandgap occurring at 0% and 50 Mol% of Cu concentration. This behaviour is attributed to the distortion induced by Cu ions, which create impurity energy levels within the bandgap of Co_3O_4[40, 41].

Photocatalytic performances of the nanocomposites

The catalytic performance of all synthesized nanocatalysts was evaluated by monitoring the decolourization of BG dye under UV light illumination, as shown in Fig. 8. The study was conducted under controlled conditions using a 100 mL BG dye solution with a concentration of 10 ppm at pH 9, with 50 mg of catalyst. As the dye solution remained under UV light illumination for an extended period, the absorption peak reduced from 625 nm to 565 nm. The photo removal of BG dye was carried out using Cu-doped Co_3O_4 and its composite with CNF. The degradation efficiencies were as follows: Pure Co_3O_4 achieved 72.2% within 50 minutes, CuCo1reached 74.5%, CuCo2 achieved 83.4%, CuCo3 reached 86.6%, CuCo4 showed 91.8%, and CuCo5 attained 89.8% within 50 minutes, as presented in Fig. 8. These findings reveal that the CuCo4 exhibits the highest photocatalytic efficiency (91.8%) within 50 min. Further research is needed for the full decolourization of the BG dye solution, leading to additional experiments with CuCo4@CNF binary nanocomposites.

Impact of CNF on the photocatalytic breakdown of BG dye

Carbon nanoflakes significantly enrich the photocatalytic decolouration of dye pollutants by improving adsorption, charge separation, light absorption, and overall catalyst stability. These enhancements lead to higher degradation efficiency and more effective treatment of organic pollutant. CNFs can act as a support material that disperses the active catalytic sites (Cu-doped Co_3O_4) more

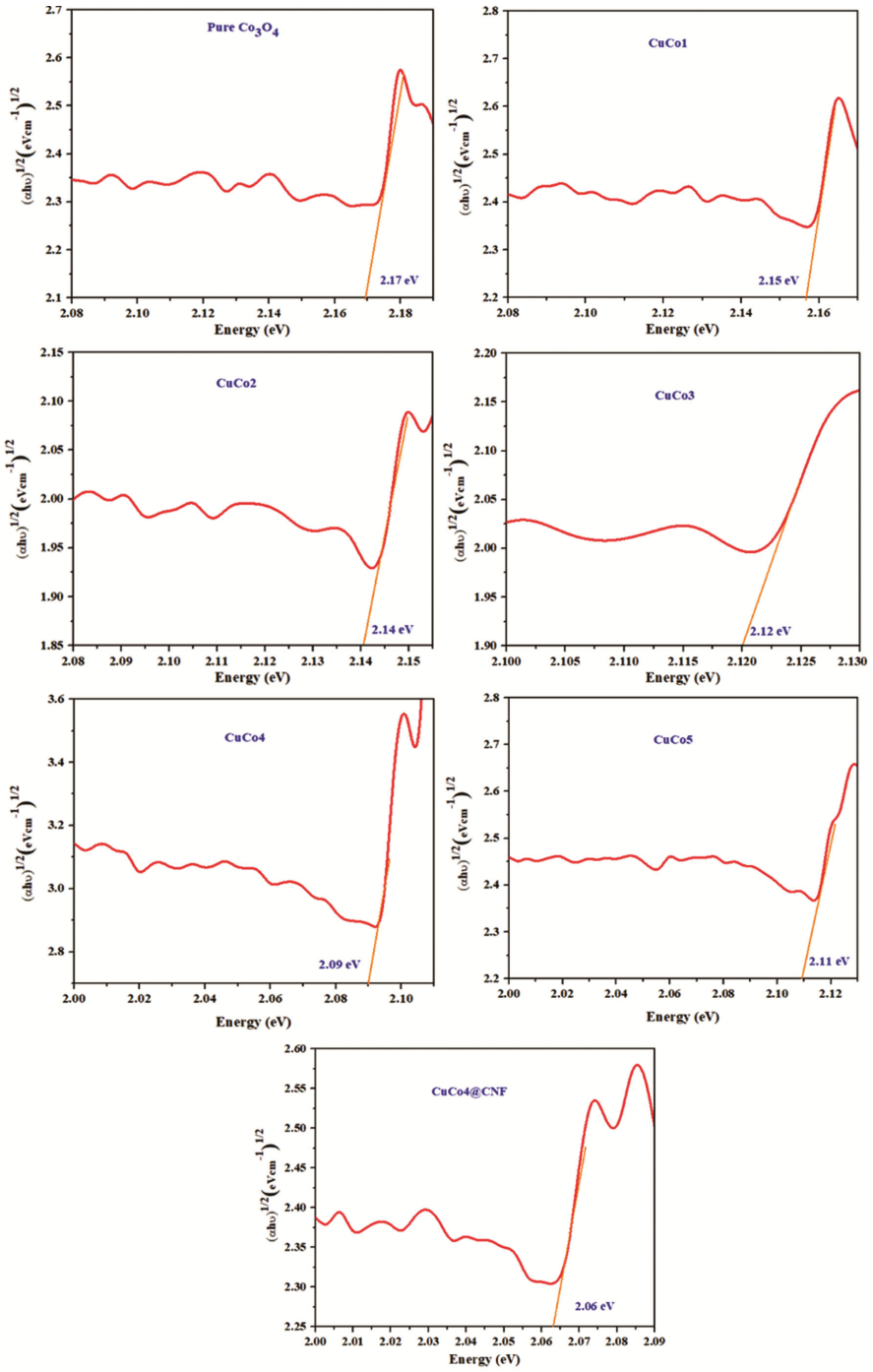

Fig. 7 — Tauc plot for all the prepared materials

effectively, preventing aggregation and ensuring major active sites are existing for the photocatalysis. The small particle size of CNF increases its surface area and provides more active adsorption sites, which enhances the adherence of BG dye molecules to the catalyst surface. This strong adsorption brings the dye molecules into closer proximity with the catalytic sites, thereby improving charge transfer efficiency and facilitating their direct interaction with the photogenerated reactive species. Consequently, the degradation process is accelerated due to the reduced diffusion distance and enhanced pollutant–catalyst contact. If CNF combines with catalytic material like CuCo4, CNFs can create synergistic effects that

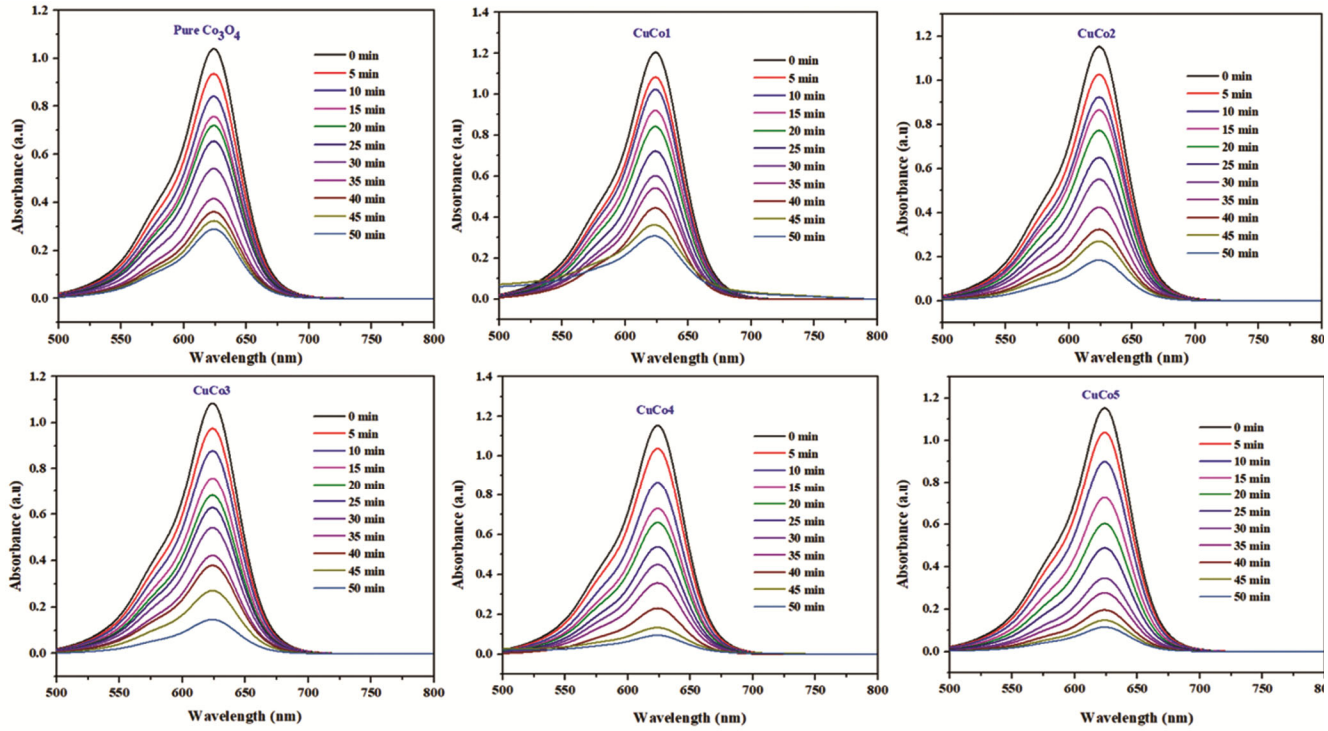

Fig. 8 — UV-visible absorption spectra of BG dye measured using different photocatalysts under UV light illumination

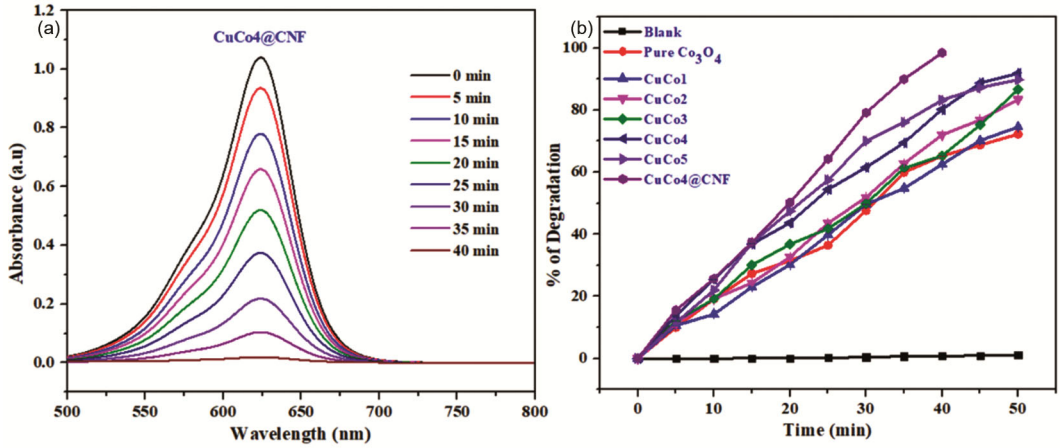

Fig. 9 — (a) UV-visible absorption spectra of BG dye using CuCo4@CNF and (b) degradation percentage of BG dye by the prepared photocatalysts

enhance the overall photocatalytic performance, and it enhances the structural stability and durability of the photocatalyst. The CuCo4@CNF nanocomposite achieved 98.4% decolourization of the BG dye solution within 40 min of UV light exposure, as depicted in Fig. 9a and 9b[26].

BG dye undergoes photocatalytic degradation under UV light illumination with a CNF-based nanocomposite, optimized by varying key factors such as catalyst dosage, solution pH, and dye concentration. The photocatalytic technique was optimized by adjusting the catalyst loading from 10 to 50 mg for the BG dye, as presented in Fig. 10a. The decolouration percentage of BG dye by the CNF-based nanocomposite at different catalyst doses (10-50 mg) for a 10-ppm dye concentration was studied. The photocatalytic removal of BG dye accelerated with the enhancing amount of catalyst. As more active sites became available, the decolouration of BG dye improved, as shown in Fig. 10a. In addition to producing more •OH radicals, the increased number of active sites on the

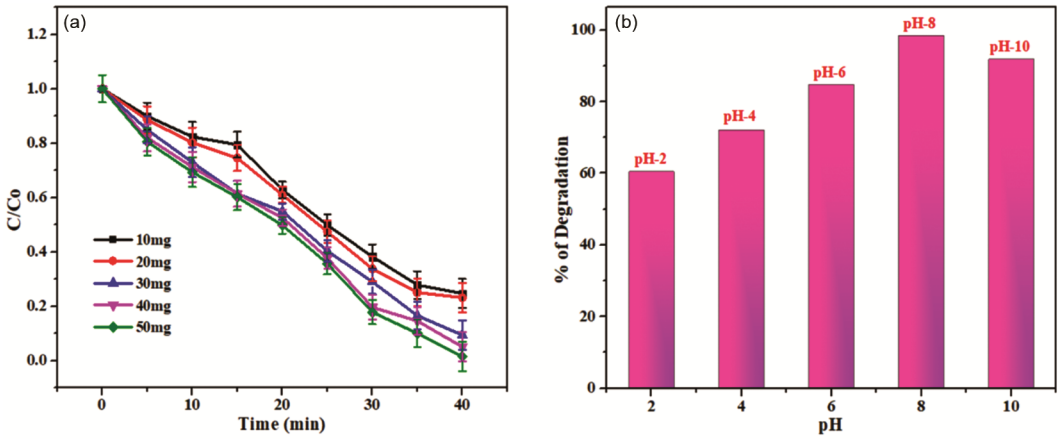

Fig. 10 — (a) Variation of catalyst loading and (b) modification of pH

photocatalyst enhances dye degradation because these sites provide more locations for pollutant molecules to adsorb and react. A higher density of active sites improves the probability of interaction between the photogenerated charge carriers (e^-/h^+ pairs) and the dye molecules, which accelerates the generation of reactive oxygen species and promotes their transfer to the pollutants. As a result, both radical availability and direct surface reactions are maximized, leading to more efficient dye degradation. Therefore, a catalyst amount of 50 mg was sufficient for the degradation process. Increasing the catalyst weight beyond the optimal level either led to saturation or slightly hindered the degradation rate. This was because higher catalyst amounts caused increased turbidity in the solution, which reduced light penetration[42].

pH plays a critical role in photocatalytic reactions, as contaminated water can vary between acidic and basic conditions. A series of experimentations were carried out with pH levels between 2 to 10, as illustrated in Fig. 10b. The initial pH was regulated using hydrochloric acid for acidic range and sodium hydroxide for alkaline range. Enhancing the pH from 2 to 8 led to a significant increase in degradation percentage under UV irradiation because pH strongly influences both the surface charge of the photocatalyst and the ionization state of the dye molecules. At acidic pH 2, strong protonation reduces the electrostatic attraction between the catalyst surface and the dye, limiting adsorption and radical attack. In contrast, at near neutral to mildly alkaline conditions 8, the catalyst surface carries more negative charge, which promotes stronger electrostatic interaction with the cationic BG dye. This improved adsorption brings the dye molecules closer to the reactive sites and enhances the formation of $^{\bullet}OH$ radicals due to higher availability of hydroxide ions (OH^-) in solution. Together, these factors result in more efficient photocatalytic degradation as illustrated in Fig. 10b. These findings indicate that pH 8.0 is the optimal condition for the photocatalytically eliminating BG dye.

The influence of the starting concentration of BG dye on the photocatalytic process was assessed by adjusting its concentration between 10 and 50 ppm under optimized conditions, as presented in Fig. 11a. The fixed catalyst amount maintains the same quantity of active sites. In the presence of high dye concentrations, BG molecules will accumulate on catalyst surfaces. However, they will be quenched as UV radiation excites these excited molecules. The quenching probability increases with higher initial dye concentration because more dye molecules act as "targets" for the photogenerated reactive, enhancing the likelihood of electron or radical transfer. However, while the initial reaction rate may be higher at elevated concentrations, the overall degradation percentage can decrease. This is because the number of dye molecules may exceed the available active sites and reactive species on the catalyst surface, and higher concentrations can also reduce UV light penetration. In contrast, at lower dye concentrations, nearly all dye molecules have access to active sites and reactive species, resulting in a higher overall degradation percentage despite a slower initial rate. In the CuCo4@CNF nanocomposite, the band gap decreased primarily due to the decrease in doping[43].

Under optimal conditions with UV irradiation, 50 mg of the nanocomposites were evaluated for reusability under 40 min of irradiation time per cycle. A pulverized nanocomposite material was permitted to settle down by gravitational force after being

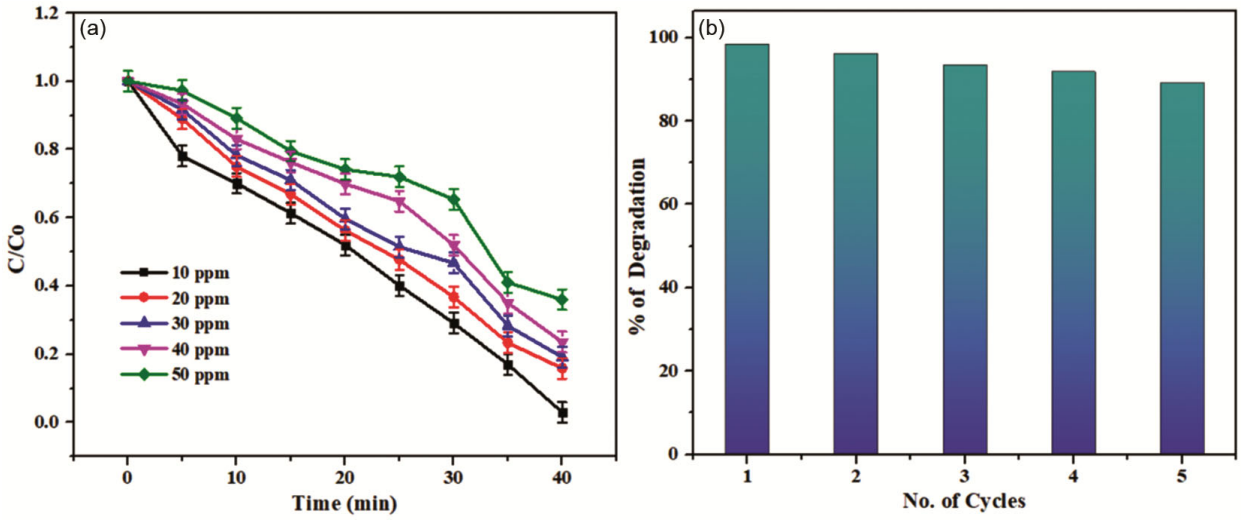

Fig. 11 — (a) BG dye removal at varying dye concentrations and (b) reuse potential of CuCo4@CNF nanocomposite

photocatalyzed degraded, then separated and collected for testing of its reusability. The reclaimed nanocomposites were reused five times under the same investigational levels. The decolouration efficiency of BG dye using CuCo4@CNF was 98.4% after the first run, 96.2% after the second run, 93.5% after the third run, 91.9% after the fourth run, and 89.2% after the fifth run was shown in Fig. 11b. The nanocomposite exhibits better stability and maintains its activity after five cycles due to its robust structural integrity and strong interaction between the active nanoparticles and the supporting matrix. The support material prevents aggregation and leaching of the nanoparticles during repeated use, preserving the active surface sites. Additionally, the nanocomposite's surface properties facilitate efficient charge separation and reduce photocorrosion under UV irradiation, allowing consistent generation of reactive species over multiple cycles. Together, these factors ensure sustained photocatalytic activity and reusability. Experimental results indicated a slight decline in the elimination percentage of BG dye with each recycling cycle of the nanocatalysts, attributed to their gradual loss of reusability. It is suggested that the CuCo4@CNF catalysts do not undergo photo erosion during photocatalytic degradation[44].

Kinetic studies

The rate constant was found out using the Eq. 4derived from the plot of ln (C_t/C_0) Vs exposure time:

$$\ln (C_t/C_0) = -kt \quad \ldots(4)$$

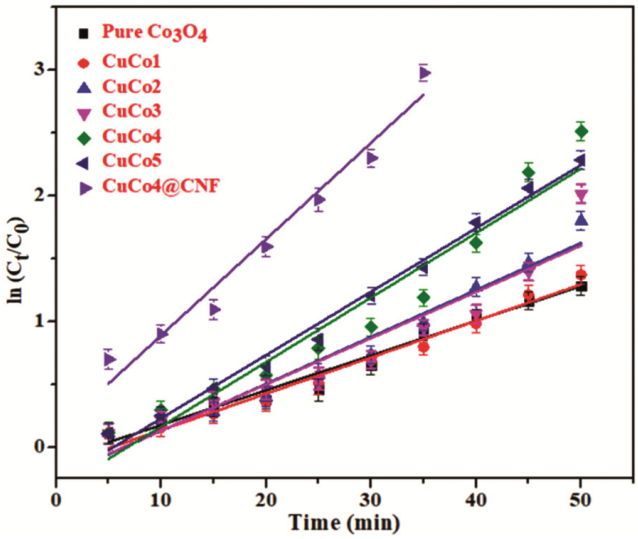

Fig. 12 — Kinetic fittings of BG dye decolouration with various catalysts.

where C_0 represents the initial concentration of BG dye, and C_t denotes the concentration at a given reaction time t. The kinetic plot (Fig. 12) exhibited a strong linear correlation coefficient (R^2), confirming that the decolorization of BG dye by CuCo4@CNF under UV light follows a pseudo-first-order kinetics model.

The rate constant (k) values were determined to 0.02764 min^{-1}, 0.02897 min^{-1}, 0.03736 min^{-1}, 0.03683 min^{-1}, 0.05134 min^{-1}, 0.05045 min^{-1} and 0.07665 min^{-1} for pure Co_3O_4, CuCo1, CuCo2, CuCo3, CuCo4, CuCo5 and CuCo4@CNF respectively. The higher rate constant reflects the superior performance of the synthesized

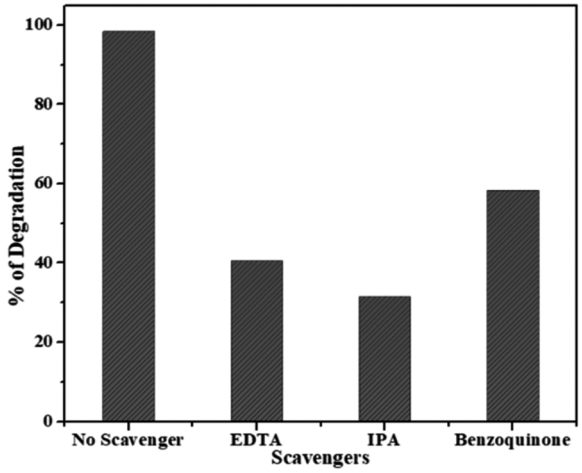

Fig. 13 — Photocatalytic elimination of BG dye in the presence of scavengers using the optimized CuCo4@CNF photocatalyst

photocatalyst because it indicates faster dye degradation under the same conditions. This is attributed to more efficient charge separation, enhanced reactive species generation, and better accessibility of active sites. Consequently, the increased rate constant directly corresponds to improved photocatalytic activity.

Photocatalytic chemistry and mechanism

The degradation of organic dyes can be accomplished photocatalytically with the help of a photocatalytic system, which absorbs enough light and converts that light into reactive oxygen species.To investigate the contribution of various reactive species in the photocatalytic reaction, disodium ethylenediaminetetraacetate (EDTA) was introduced to capture holes (h^+), benzoquinone (BQ) was used as a superoxide radical ($^{\bullet}O_2^-$) scavenger, and isopropyl alcohol (IPA) was added to trap hydroxyl radicals ($^{\bullet}OH$). Notably, in the absence of scavengers, 98.4% removal efficiency was achieved, because all the photogenerated reactive species are freely available to interact with the dye molecules. Without scavengers, there is no inhibition or competition for these species, allowing maximum electron or radical transfer to the pollutant. This unhindered reaction leads to efficient dye degradation and explains the observed high removal efficiency, as indicated in Fig. 13. The photocatalytic elimination of BG was reduced with IPA and EDTA, suggesting that photo induced holes generated during UV light absorption by the catalyst serves a key function in producing of h^+ and OH^-radicals. These radicals are the main contributors to the efficient removal of the organic dye molecules[45], or they may be formed through the reaction between adsorbed H_2O molecules and h^+[46].

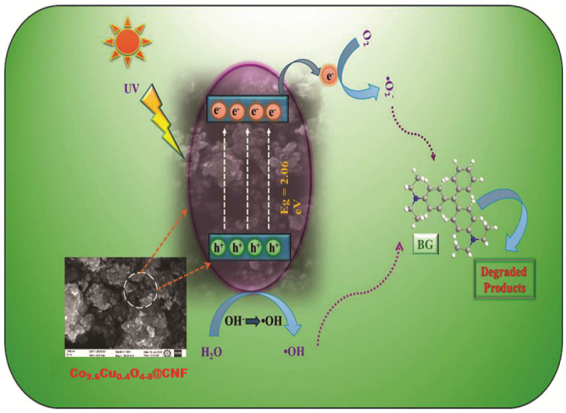

Fig. 14 — Diagrammatic illustration of the photocatalytic degradation mechanism of BG dye using CuCo4@CNF

Plausible mechanism

Fig. 14 shows the plausible mechanism for photocatalytic degradation of BG dye using CNF-based nanocomposite materials[46]. The reaction sequences are described below:

$$Co_3O_4 + \text{Light} \rightarrow Co_3O_4\,(h^+_{VB}) + Co_3O_4\,(e^-_{CB}) \quad \ldots(5)$$

$$Co_{2.60}Cu_{0.40}O_{4-\delta}@CNF + \text{Light} \rightarrow CNF\,(e^-) \quad \ldots(6)$$

$$(e^-_{CB}) + O_2 \rightarrow {}^{\bullet}O_2^- \quad \ldots(7)$$

$$(h^+_{VB}) + OH \rightarrow {}^{\bullet}OH \quad \ldots(8)$$

$$^{\bullet}OH + {}^{\bullet}O_2^- + BG \rightarrow \text{Degradation products} \quad \ldots(9)$$

Under UV light exposure, electrons in CuCo4@CNF transition from the valence band (VB) to the conduction band (CB), leading to the generation of positive holes (h^+) in the VB and electrons (e^-) in the CB. The VB and CB of Co_3O_4/CuO facilitate the formation of hydroxyl (•OH) and superoxide ($^{\bullet}O_2^-$) radicals due to the presence of strong oxidizing and reducing agents. It is essential to point out that CNF captures the photogenerated electrons, giving rise to the production of ROS in the CNF photocatalyst, such as O_2 and OH radicals. In an environment of ultraviolet light, ROS is the major source for the elimination of the BG dye molecule. It may be possible that the CNF composite material, which has a lower bandgap than other synthesized materials, is better suited to use UV light to break down BG dye than other prepared samples. Consequently, the CNF composite has a smaller bandgap, which reduces the recombination proportion of holes and electrons. By reacting with dye molecules, ROS produces degradable products such as CO_2 and water (Eqs (5-9))[26, 55]. The efficiency of cobalt oxide-based materials in the photocatalytic degradation of different organic dyes is presented in Table 2.

Table 2 — Efficiency of cobalt oxide-based materials in the photocatalytic degradation of different organic dyes.

S. No.	Name of the catalyst	Synthesis method	Dye used	% of Degradation	Time (min)	Light Source Used	Reference
1	Co_3O_4, Citric acid capped Co_3O_4 and Oleic acid capped Co_3O_4	Sol-gel	MG	47.7 91.2 66.6	100	-	Verma *et al.*[47]
2	Co and Co_3O_4 NP	Microwave and Reductive chemical heating	EBT and Murexide	89.4 and 43.6	40	Sun	Adekunle *et al.*[48]
3	Cobalt substituted cubic NiO NP	Facile Co-precipitation	MB	94	50	Visible	Khatri & Rana[49]
4	Co_3O_4	Green Synthesis	Acid Blue-74	98	150	UV	Samuel *et al.*[50]
5	Co_3O_4	Sol-gel	MB	93.8	90	Visible	Vennela *et al*.[31]
6	Co_3O_4	Hydrothermal	MV and CV	92 and 64	45	UV	Saravan *et al*.[51]
7	Co_3O_4	Sol-gel	RhB and DR-80	32 and 78	180	Visible	Dhas*et al.*[52]
8	Co_3O_4/ZnO	Facile low-temperature solution process	RhB	98	50	UV	Kumar *et al.*[53]
9	EDTA supported Co_3O_4	Sol-gel	MG and CV	56.3 and 37.9	100 and 190	Visible	Singh *et al.*[54]
10	Pure Co_3O_4 CuCo4 CuCo4@CNF	Chemical Co-precipitation method	BG		50 50 40	UV	Present work

Conclusion

Pure cobalt oxide, copper-doped cobalt oxide, and carbon nanoflake-based Co_3O_4 nanoparticles were effectively fabricated through an uncomplicated soft chemical approach. The prepared samples underwent extensive analytical characterization. The materials incorporating CNF displayed a distinct flake-like structure and outstanding optical properties, with a bandgap energy of 2.06 eV. These nanocomposites were found to be effective in wastewater purification. All synthesized nanomaterials were successfully applied to eliminate BG dye molecules from water. Among them, the CNF-based Cu-doped cobalt oxide nanocomposite exhibited higher degradation efficiency (98.4% within 40 min) in degrading brilliant green compared to pure Co_3O_4 and Cu-doped Co_3O_4 nanoparticles, attributed to the reduced bandgap and CNF having higher surface area. To efficiently degrade the dye, it is more beneficial to use lower dye concentrations and higher catalyst doses at the start of the process.

Acknowledgements

The authors would like to thank Kalasalingam Academy of Research and Education for providing the facilities to carry-out this research work. Mr. R. Sathish Kannan is gratefully acknowledged for his help in UV measurements.

Conflict of interest

The authors declare no conflict of interest.

References

1 Sriram G, Bendre A, Mariappan E, Altalhi T, Kigga M, Ching Y C, Jung H Y, Bhaduri B & Kurkuri M, Recent trends in the application of metal-organic frameworks (MOFs) for the removal of toxic dyes and their removal mechanism-A review, *Sustain Mater Technol*, 31 (2022) e00378.

2 Nandi B K, Goswami A & Purkait M K, Adsorption characteristics of brilliant green dye on kaolin, *J Hazard Mater*, 161 (2009) 387.

3 Rehman F, Sayed M, Khan J A, Shah N S, Khan H M & Dionysiou D D, Oxidative removal of brilliant green by UV/$S_2O_8^{2-}$,UV/HSO^5-and UV/H_2O_2 processes in aqueous media: A comparative study, *J Hazard Mater*, 357 (2018) 506.

4 Zheng Y, Yao G, Cheng Q, Yu S, Liu M & Gao C, Positively charged thin-film composite hollow fiber nanofiltration membrane for the removal of cationic dyes through submerged filtration, *Desalination*, 328 (2013) 42.

5 Tripathy B K, Kumar S, Kumar M & Debnath A, Microwave induced catalytic treatment of brilliant green dye with carbon doped zinc oxide nanoparticles: Central composite design, toxicity assessment and cost analysis, *Environ Nanotechnol Monit Manag*, 14 (2020) 100361.

6 Tripathy B K & Kumar M, Suitability of microwave and microwave-coupled systems for landfill leachate treatment: An overview, *J Environ Chem Eng*, 5 (2017) 6165.

7 Singh N H, Kezo K, Debnath A & Saha B, Enhanced adsorption performance of a novel Fe-Mn-Zr metal oxide nanocomposite adsorbent for anionic dyes from binary dye

mix: Response surface optimization and neural network modelling, *Appl Organomet Chem*, 32 (2018) e4165.
8 Nandi B K & Patel S, Removal of brilliant green from aqueous solution by electrocoagulation using aluminum electrodes: Experimental, kinetics, and modeling, *Sep Sci Technol*, 49 (2014) 601.
9 Rao C V, Giri A S, Goud V V & Golder A K, Studies on pH-dependent color variation and decomposition mechanism of Brilliant Green dye in Fenton reaction, *Int J Ind Chem*, 7 (2016) 71.
10 Safajou H, Khojasteh H, Salavati-Niasari M & Mortazavi-Derazkola S, Enhanced photocatalytic degradation of dyes over graphene/Pd/TiO_2 nanocomposites: TiO_2 nanowires versus TiO_2 nanoparticles, *J Colloid Interf Sci*, 498 (2017) 423.
11 Mahdiani M, Soofiv F, Ansari F & Salavati-Niasari M, Grafting of $CuFe_{12}O_{19}$ nanoparticles on C.N.T. and graphene: Ecofriendly synthesis, characterization and photocatalytic activity, *J Clean Prod*, 176 (2018) 1185.
12 Dammala P, Machado J, Rani B, Murali S, Devi S, Luwang M N & Sahu N K, Synthesis of biphasic nanomaterials based on ZnO and SnO_2: Application towards photocatalytic degradation of acid red dye, *Nano-Struct Nano Objects*, 18 (2019) 100292.
13 Sujatha K, Seethalakshmi T, Sudha A P & Shanmugasundaram O L, Photocatalytic activity of pure, Zn doped and surfactants assisted Zn doped SnO_2 nanoparticles for degradation of cationic dye, *Nano Struct Nano Objects*, 18 (2019) 100305.
14 Maniammal K, Madhu G & Biju V, Nanostructured mesoporous NiO as an efficient photocatalyst for degradation of methylene blue: Structure, properties and performance, *Nano Struct Nano Objects*, 16 (2018) 266.
15 Chan S H S, Wu T Y, Juan J C & Teh C Y, Recent developments of metal oxide semiconductors as photocatalysts in advanced oxidation processes (AOPs) for treatment of dye waste-water, *J Chem Technol Biotechnol*, 86 (2011) 1130.
16 Hamdani M, Singh R N & Chartier P, Co_3O_4 and Co-based spinel oxides bifunctional oxygen electrodes, *Int J Electrochem Sci*, 5 (2010) 556.
17 Barakat N A M, El-Newehy M, Al-Deyab S S & Kim H Y, Cobalt/copper-decorated carbon nanofibers as novel non-precious electrocatalyst for methanol electrooxidation, *Nanoscale Res Lett*, 9 (2014) 2.
18 Adekunle A S & Ozoemena K I, Electrosynthesised metal (Ni, Fe, Co) oxide films on single-walled carbon nanotube platforms and their supercapacitance in acidic and neutral pH Media, *Electroanalysis*, 23 (2011) 971.
19 Obisesan O R, Adekunle A S, Oyekunle J A O, Sabu T, Nkambule T T I & Mamba B B, Development of electrochemical nanosensor for the detection of malaria parasite in clinical samples, *Front Chem*, 7 (2019) 89.
20 Xie X & Shen W, Morphology control of cobalt oxidenanocrystals for promoting their catalytic performance, *Nanoscale*, 1 (2009) 50.
21 Mai H X, Sun L D, Zhang Y W, Si R, Feng W, Zhang H P, Liu H C & Yan C H, Shape-selective synthesis and oxygen storage behavior of ceria nanopolyhedra, nanorods, and nanocubes, *J Phys Chem B*, 109 (2005) 24380.
22 Azhdari F & Ghaz M M, Photocatalytic degradation of textile dye direct orange 26 by using $CoFe_2O_4/Ag_2O$, *Adv Environ Technol*, 2 (2016) 77.
23 El-Bahy Z M, Mohamed M M, Zidan F I & Thabet M S, Photo-degradation of acid green dye over Co-ZSM-5 catalysts prepared by incipient wetness impregnation technique, *J Hazard Mater*, 153 (2008) 364.
24 Narde S B, Lanjewar R B, Gadegone S M & Lanjewar M R, Photocatalytic degradation of azo dye congo red using $Ni_{0.6}Co_{0.4}Fe_2o_4$ as photocatalyst, *Der Pharma Chemica*, 9 (2017) 115.
25 Sharma O & Sharma M K, Use of cobalt hexacyanoferrate(II) semiconductor In photocatalytic degradation of neutral red dye, *Int J Chem Tech Res*, 5 (2013) 1615.
26 Vinayagasundaram C & Nesaraj A S, Surfactant assisted wet chemical synthesis of Cu doped NiO@CNF nanocomposites and their photocatalytic behaviour in degrading brilliant green dye under UV light irradiation, *Inorg Chem Commun*, 168 (2024) 112867.
27 Vinayagasundaram C, Samson N A & Sivaranjana P, Overview on multicomponent ceramic composite materials used for efficient photocatalysis-An update, *J Indian Chem Soc*, 100 (2023) 100908.
28 Mukhtar M, Munisa L & Saleh R, Co-precipitation synthesis and characterization of nanocrystalline zinc oxide particles doped with Cu_2+ions, *Mater Sci Appl*, 3 (2012) 543.
29 Esquivel K, Garc M G, Rodr F J, Ortiz-Frade L A & Godinez L A, Study of the photo-electrochemical activity of cobalt- and nickel-doped TiO_2 photo-anodes for the treatment of a dye-contaminated aqueous solution, *J Appl Electrochem*, 43 (2013) 433.
30 Sharifi S L, Shakur H R, Mirzaei A & Hosseini M H, Characterization of cobalt oxide Co_3O_4 nanoparticles prepared by various methods: Effect of calcination temperatures on size, dimension and catalytic decomposition of hydrogen peroxide, *Int J Nanosci Nanotechnol*, 9 (2013) 51.
31 Vennela A B, Mangalaraj D, Muthukumarasamy N, Agilan S & Hemalatha K V, Structural and optical properties of Co_3O_4 nanoparticles prepared by sol-gel technique for photocatalytic application, *Int J Electrochem Sci*, 14 (2019) 3535.
32 Karthick S N, Hemalatha K V, Justin R C, Kim H J & Yi M, Synthesis of nano-bound microsphere Co_3O_4 by simple polymer-assisted sol-gel technique, *J Nanopart Res*, 15 (2013) 1474.
33 Luo X, Huang M, Bie L, He D, Zhang Y & Jiang P, $CuCo_2O_4$ nanowire arrays supported on carbon cloth as an efficient 3D binder-free electrode for non-enzymatic glucose sensing, *Rsc Adv*, 7 (2017) 23093.
34 Jeghan S M N & Kang M, Facile synthesis and photocatalytic activity of cubic spinel urchin-like copper cobaltite architecture, *Mater Res Bull*, 91 (2017) 108.
35 Tougaard S & Tahir D, Electronic and optical properties of Cu, CuO and Cu2O studied by electron spectroscopy, *J Phys Condens Mater*, 24 (2012) 175002.
36 Liu S, Hui K & Hui K, Flower-like copper cobaltite nanosheets on graphite paper as high-performance supercapacitor electrodes and enzymeless glucose sensors, *ACS Appl Mater Interf*, 8 (2016) 3258.

37 Qiu K, Lu M, Luo Y & Du X, Engineering hierarchical nanotrees with $CuCo_2O_4$ trunks and NiO branches for high-performance supercapacitors, *J Mater Chem A*, 5 (2017) 5820.

38 Li H, Fei G T, Fang M, Cui P, Guo X, Yan P & Li Z D, Synthesis of urchin-like Co_3O_4 hierarchical micro/nanostructures and their photocatalytic activity, *Appl Surf Sci*, 257 (2011) 6527.

39 Senthilkumar N, Vivek E, Shankar M, Meena M, Vimalan M & Potheher I V, Synthesis of ZnO nanorods by one step microwave-assisted hydrothermal route for electronic device applications, *J Mater Sci-Mater Elect*, 29 (2018) 2927.

40 Zahan M & Podder J, Synthesis and characterizations of Cu doped Co_3O_4 nanostructured thin films using spray pyrolysis for glucose sensor applications, *Biointerf Res Appl Chem*, 12 (2022) 6321.

41 Ali G A M, Fouad O A & Makhlouf S A, Structural, optical and electrical properties of sol-gel prepared mesoporous Co_3O_4/SiO_2 nanocomposites, *J Alloys Compd*, 579 (2013) 606.

42 Sharma A & Lee B K, Adsorptive/photo-catalytic process for naphthalene removal from aqueous media using in-situ nickel doped titanium nanocomposite, *J Environ Manag*, 155 (2015) 114.

43 Khairnar S D, Patil M R & Shrivastava V S, Hydrothermally synthesized nanocrystalline Nb_2O_5 and its visible-light photocatalytic activity for the degradation of congo red and methylene blue, *Iran J Catal*, 8 (2018) 143.

44 Patil S P, Patil R P, Mahajan V K, Sonawane G H & Shrivastava V S, Facile sonochemical synthesis of Bio Br-graphene oxide nanocomposite with enhanced photocatalytic activity for the degradation of Direct green, *Mater Sci Semicond Process*, 52 (2016) 55.

45 Deng W, Zhao H, Pan F, Feng X, Jung B, Abdel-Wahab A, Batchelor B & Li Y, Visible-light-driven photocatalytic degradation of organic water pollutants promoted by sulfite addition, *Environ Sci Technol*, 51 (2017) 13372.

46 Neta P & Huie R E, Free-radical chemistry of sulphite, *Environ Health Perspect*, 64 (1985) 209.

47 Verma M, Mitan M, Kim H & Vaya D, Efficient photocatalytic degradation of Malachite green dye using facilely synthesized cobalt oxide nanomaterials using citric acid and oleic acid, *J Phys Chem Solids*, 155 (2021) 110125.

48 Adekunle A S, Oyekunle J A O, Durosinmi L M, Oluwafemi O S, Olayanju D S, Akinola A S, Obisesan O R, Akinyele O F & Ajayeoba T A, Potential of cobalt and cobalt oxide nanoparticles as nanocatalyst towards dyes degradation in wastewater, *Nano Struct Nano Objects*, 21 (2020) 100405.

49 Khatri A & Rana P S, Visible light photocatalysis of methylene blue using cobalt substituted cubic NiO nanoparticles, *Bull Mater Sci*, 42 (2019) 141.

50 Samuel M S, Selvarajan E, Mathimani T, Santhanam N, Phuong T N, Brindhadevi K & Pugazhendhi A, Green synthesis of cobalt-oxide nanoparticle using jumbo Muscadine (*Vitis rotundifolia*): Characterization and photo-catalytic activity of acid Blue-74, *J Photochem Photobiol B: Biol*, 211 (2020) 112011.

51 Saravan R S, Muthukumaran M, Mubashera S M, Abinaya M, Prasath P V, Parthiban R & Sagadevan S, Evaluation of the photocatalytic efficiency of cobalt oxide nanoparticles towards the degradation of crystal violet and methylene violet dyes, *Optik*, 207 (2019) 164428.

52 Dhas C R, Venkatesh R, Jothivenkatachalam K, Nithya A, Benjamin B S, Raj A M E & Sanjeeviraja C, Visible light driven photocatalytic degradation of Rhodamine B and Direct Red using cobalt oxide nanoparticles, *Ceram Int*, 41 (2015) 9301.

53 Kumar R, Umar A, Kumar R, Chauhan M S, Kumar G & Chauhan S, Spindle-like Co_3O_4-ZnO nanocomposites scaffold for hydrazine sensing and photocatalytic degradation of Rhodamine B dye, *Eng Sci*, 16 (2021) 288.

54 Singh M, Vaya D, Kumar R & Das B, Role of EDTA capped cobalt oxide nanomaterial in photocatalytic degradation of dyes, *J Serb Chem Soc*, 86 (2021) 327.

55 Kalam A, Al-Sehemi A G, Assiri M, Du G, Ahmad T, Ahmad I & Pannipara M, Modified solvothermal synthesis of cobalt ferrite ($CoFe_2O_4$) magnetic nanoparticles photocatalysts for degradation of methylene blue with H_2O_2/visible light, *Results Phys*, 8 (2018) 1046.